Applied Catalysis B: Environmental 245 (2019) 569–582

Contents lists available at ScienceDirect

Applied Catalysis B: Environmental

journal homepage: www.elsevier.com/locate/apcatb

# Facile and green synthetic strategy of birnessite-type $MnO_2$ with high efficiency for airborne benzene removal at low temperatures

Yang Liu[a,*], Hao Zhou[a], Ranran Cao[b], Xingyun Liu[a], Pengyi Zhang[b,*], Jingjing Zhan[a], Lifen Liu[a]

[a] Key Laboratory of Industrial Ecology and Environmental Engineering (Ministry of Education), School of Food and Environment, Dalian University of Technology, Panjin, 124221, China

[b] School of Environment, Tsinghua University, Beijing, 100084, China

ARTICLE INFO

*Keywords:*
Catalytic oxidation
VOCs
Benzene
Manganese oxide
Water resistance

ABSTRACT

Volatile organic compounds (VOCs) are notorious for global air pollution. It is key to find a material with high and stable activity to catalytically oxidize VOCs at low temperatures. In this paper, benzene, as a typical VOC contaminant, could be completely oxidized on a highly efficient and moisture-resistant birnessite $MnO_2$ at temperatures significantly lower than the reported values in literature. The best catalyst (H-$MnO_2$ (30-0.2-6)) could be tailored via a facile and green process by engineering a proper combination of treatment temperature (30 °C), $HNO_3$ aqueous concentration (0.2 M) and treatment period (6 h). The thus-obtained $MnO_2$ exhibited a stable removal efficiency of ~94% for 318 ppm of benzene under a high space velocity of 120 $L{\cdot}g^{-1}\,h^{-1}$ and 1.5 vol.% $H_2O$ at 250 °C. XRD, SEM, (HR)TEM, EDS mapping, XPS, $H_2$-TPR, $O_2$-TPD and pyridine adsorption IR were combined with the deliberately designed $C_6H_6$-TPD, surface oxidation reaction of benzene and $CO_2$-TPD to disclose the tremendous role of acid treatment in benzene oxidation. The increased acid sites and acidity of the acid-treated surface promoted the adsorption and activation of gaseous benzene, and the lattice oxygen and surface adsorbed oxygen became more facile and reactive due to the generated active oxygen vacancies via acid treatment, these two favorable factors together with the easy desorption of reaction products resulting in the excellent performance of the acid-treated sample. Finally, the acid treatment method can be extended to most of other crystal structures of manganese dioxides except α-$MnO_2$.

## 1. Introduction

According to the annual report of the *State of Global Air 2018* [1], air pollution is the leading environmental cause of death worldwide and is the 4th highest cause of death among all health risks, especially in the developing countries. For example, China and India now are among the highest air pollution health burdens in the world. Volatile organic compounds (VOCs) are notorious for the global air pollution. They are also the precursors of ozone, photochemical smog and secondary aerosols [2]. As one of the most abundant VOCs in polluted air, benzene is extremely difficult to decompose and can transport in a long distance, which is posing a great threat to human health and environmental development. As released by the World Health Organization [3], human exposure to benzene has been associated with a range of acute and long-term adverse health effects and diseases, including cancer and aplastic anaemia, *etc*. Exposure can occur as a result of the ubiquitous use of benzene-containing petroleum products, including motor fuels and solvents; besides, people spending more time indoors are likely to have higher exposure to benzene due to decorative materials [3].

Hitherto, catalytic oxidation at elevated temperatures has been generally considered as an efficient method to eliminate benzene pollution [4]. And the development of high-performance catalysts is the key issue. For industrial discharging, the catalyst can be coated on to various substrates, such as ceramic honeycomb, cordierite monolith and metal mesh, *etc*., and the thermal decomposition of residual benzene can be achieved by utilizing the waste heat of the industrial processes; for residential indoor air, although ventilation is a good choice, haze weather that erupts in recent years does not allow people to do so, therefore, it is a good alternative to apply the catalyst to the filter element of an air purifier. The development of noble metals [5–10] and transition metal oxides [11–16] for benzene oxidation has been widely reported in literature. However, the practical application of noble metals is severely hindered by their prohibitively high cost. Benzene oxidation reactions over non-precious metal oxides are mainly focused on the oxides of Cu [11,15], Co [11], Ti [12], V [11,12], Mo [11,13], W [13], Ce [16] and Mn [11,14], *etc*. Usually catalyst deactivation [17]

* Corresponding authors.
*E-mail addresses:* liuyang20180129@dlut.edu.cn (Y. Liu), zpy@tsinghua.edu.cn (P. Zhang).

https://doi.org/10.1016/j.apcatb.2019.01.023
Received 25 October 2018; Received in revised form 23 December 2018; Accepted 9 January 2019
Available online 09 January 2019
0926-3373/ 

due to the coexistence of water vapor and other pollutants, *e.g.*, nitrogen compounds, organohalogens and sulfur compounds, *etc.*, is one of the main obstacles restricting their practical uses.

Manganese oxide minerals are ubiquitous in nature, and they are commonly found in terrestrial deposits and ocean nodules [18]. Typically, manganese oxide minerals can be divided into two categories according to the arrangement of the [$MnO_6$] octahedra, *i.e.*, the tunnel structure (such as β-$MnO_2$, γ-$MnO_2$, α-$MnO_2$ and todorokite $MnO_2$, *etc.*, with 1 × 1, 1 × 2, 2 × 2 and 3 × 3 tunnel, respectively) and layer structure (birnessite $MnO_2$ or δ-$MnO_2$). Birnessite $MnO_2$, which is consisted of sheets of edge-sharing [$MnO_6$] octahedra with an interlayer space of ~7 Å [19], has been paid much attention in the field of catalysis [20–24]. However, when it comes to benzene oxidation, there are only a few reports using birnessite $MnO_2$ as catalysts. Li et al. [25] hydrothermally prepared three birnessite $MnO_2$ with different morphologies, and found that the birnessite nanoflowers, which possessed the highest concentration of oxygen vacancies, were the most active for benzene oxidation. Ye and Dai et al. [26] also investigated the effect of morphology of birnessite $MnO_2$ on benzene oxidation, and they concluded that the Mn oxide nature, surface lattice oxygen mobility and reducibility were the key factors influencing the catalytic performance. Chen et al. [27] hydrothermally prepared birnessite $MnO_2$ and investigated the effect of Ti doping on benzene oxidation. Thanks to the active oxygen induced by Ti doping and the abundant pore structures, the Ti-doped sample possessed higher activity. In our previous study [28], the tremendous catalytic enhancement resulted from the exchange of interlayer $K^+$ of birnessite $MnO_2$ by $Cu^{2+}$ was reported to be related to the easier reducibility and the higher lattice oxygen reactivity of the Cu-exchanged sample. Although progress has been made in benzene oxidation by using birnessite $MnO_2$, the catalytic activity and stability at low reaction temperatures (100–200 °C), especially under humid reaction condition, still need improving from the viewpoints of energy saving, lowering operation costs and safety, and the conclusions drawn from birnessite $MnO_2$ have important implications for the development of other kinds of benzene oxidation materials. Herein, redox reaction between $KMnO_4$ and methanol at low temperature and atmospheric pressure was adopted to fabricate birnessite $MnO_2$, which was further treated by $HNO_3$ aqueous solution at room temperature to obtain efficient and water resistant benzene oxidation material with long-term stability at relatively low reaction temperatures. Acid treatment did not change the crystal structure of birnessite, and this process was GREEN since the $HNO_3$ solution could be recycled over times. More importantly, acid treatment method can be extended to most of other crystalline $MnO_2$ catalysts. Finally, comparative characterizations of the physicochemical properties of the catalysts before and after acid treatment together with the temperature programmed desorption of adsorbed benzene and $CO_2$ and surface oxidation reaction of benzene were performed to explore the intrinsic mechanism of the enhancement of catalytic benzene oxidation by acid treatment.

## 2. Experimental

### 2.1. Catalyst synthesis and characterization

All the reagents were used as received without further treatment. The birnessite-type $MnO_2$, which was obtained through the redox reaction between $KMnO_4$ and $CH_3OH$ solution, was denoted as *pristine $MnO_2$*. Briefly, an appropriate amount of $KMnO_4$ solid was fully dissolved in deionized water. Then $CH_3OH$ was added into the $KMnO_4$ solution under constant stirring by magnetic stirrer and the mixture was kept stirring for 12 h. After filtration and washing with deionized water, the obtained solid was dried at 105 °C overnight in an oven.

Subsequently, the pristine $MnO_2$ powder was soaked in $HNO_3$ solution in a beaker and constantly stirred in a water bath. The mass ratio of solid to liquid was fixed at 1:20. The effects of $HNO_3$ aqueous concentration, treatment temperature and treatment period were investigated. After acid treatment, the suspension was filtered and repeatedly washed with deionized water until the pH of the eluate was ~7.0. The resultant solid was then dried at 105 °C overnight in an oven. The obtained powder was grounded, tableted, crushed and sieved to 40–60 mesh. For convenience, the acid-treated $MnO_2$ was denoted as *H-$MnO_2$ (T-C-t)*, where *T*, *C* and *t* represent the treatment temperature (°C), $HNO_3$ aqueous concentration (M) and treatment period (h), respectively.

In order to test the universality of the $HNO_3$ treatment method for other $MnO_2$ materials, the pristine β-$MnO_2$ (1 × 1 tunnel), α-$MnO_2$ (2 × 2 tunnel) and todorokite $MnO_2$ (3 × 3 tunnel) were prepared according to reference [29–31], respectively, and a commercial $MnO_2$ (CAS: 1313-13-9) purchased from the Aladdin company was also used. The acid treatment of these four samples was carried out under the optimal conditions (*T*, *C* and *t*) obtained from the birnessite $MnO_2$.

For details of the instruments, procedures and parameters used for the characterizations of the surface and bulk properties of the catalysts, see the electronic supplementary information.

### 2.2. Gaseous benzene oxidation

Catalytic benzene oxidation was performed in a continuous-flow fix-bed quartz tube reactor with an inner diameter of 6 mm loaded with ~0.1 g of catalyst under atmospheric pressure. 200 mL·min$^{-1}$ of synthetic air (20 vol.% $O_2$ + 80 vol.% $N_2$) containing 300–400 ppm of benzene was fed into the catalyst bed, corresponding to a space velocity of ~120 L·g$^{-1}$ h$^{-1}$. After the adsorption-desorption-reaction equilibrium of benzene was achieved at one temperature on the catalyst surface, the catalyst was heated up with a rate of 5 °C·min$^{-1}$ to the next set temperature. Water vapor was generated by flowing synthetic air through a water bubbler at 26 °C, and the humid air was then mixed with the dry air flow containing benzene. The outlet benzene concentration was monitored online by VOCs detector (MiniRAE 3000, USA), and benzene conversion was calculated according to the difference between the inlet and outlet benzene concentrations.

### 2.3. Temperature programmed desorption of adsorbed benzene ($C_6H_6$-TPD), $O_2$-TPD, surface oxidation reaction of benzene ($C_6H_6$-SOR) and $CO_2$-TPD

The interaction between benzene molecules and catalyst surface was evaluated by $C_6H_6$-TPD. About 0.1 g of catalyst was used for $C_6H_6$-TPD. 200 mL·min$^{-1}$ of $N_2$ with ~380 ppm of benzene flowed through the catalyst bed. After adsorption for 1 h, 200 mL·min$^{-1}$ of pure $N_2$ was switched into the reactor to purge the physically absorbed benzene molecules, and then the sample was heated at a rate of 10 °C·min$^{-1}$ to 400 °C in the same atmosphere. The desorbed benzene was detected by the VOCs detector.

$O_2$-TPD is useful to quantify the relative amounts of surface oxygen species and characterize their activities. $O_2$-TPD was performed on Chemisorption Analyzer (Autochem II 2920, Micromeritics, USA). After pretreated in 50 mL·min$^{-1}$ of helium at 105 °C for 30 min and then cooled down to 40 °C, the ~0.05 g of catalyst was subject to 30-min $O_2$ adsorption with 50 mL·min$^{-1}$ of 5 vol.% $O_2$/He. After purged by 50 mL·min$^{-1}$ of helium for 30 min to desorb the physiosorbed $O_2$, the catalyst was heated in the same atmosphere with a ramp of 10 °C·min$^{-1}$. The impurities were removed by a cold trap at −80 °C before the outlet flow entered the thermal conductivity detector.

The $C_6H_6$-SOR was adopted to assess the activity of the catalyst surface to activate gaseous oxygen for benzene oxidation. The dynamic switching between air and benzene was carried out as follows: first, the catalyst was activated in 100 mL·min$^{-1}$ of synthetic air at 350 °C or 200 °C for 30 min; then, 200 mL·min$^{-1}$ of $N_2$ with ~380 ppm of benzene was led into the reactor to initiate benzene oxidation by surface oxygen species. These procedures were repeated several times. The outlet benzene was monitored by the VOCs detector.

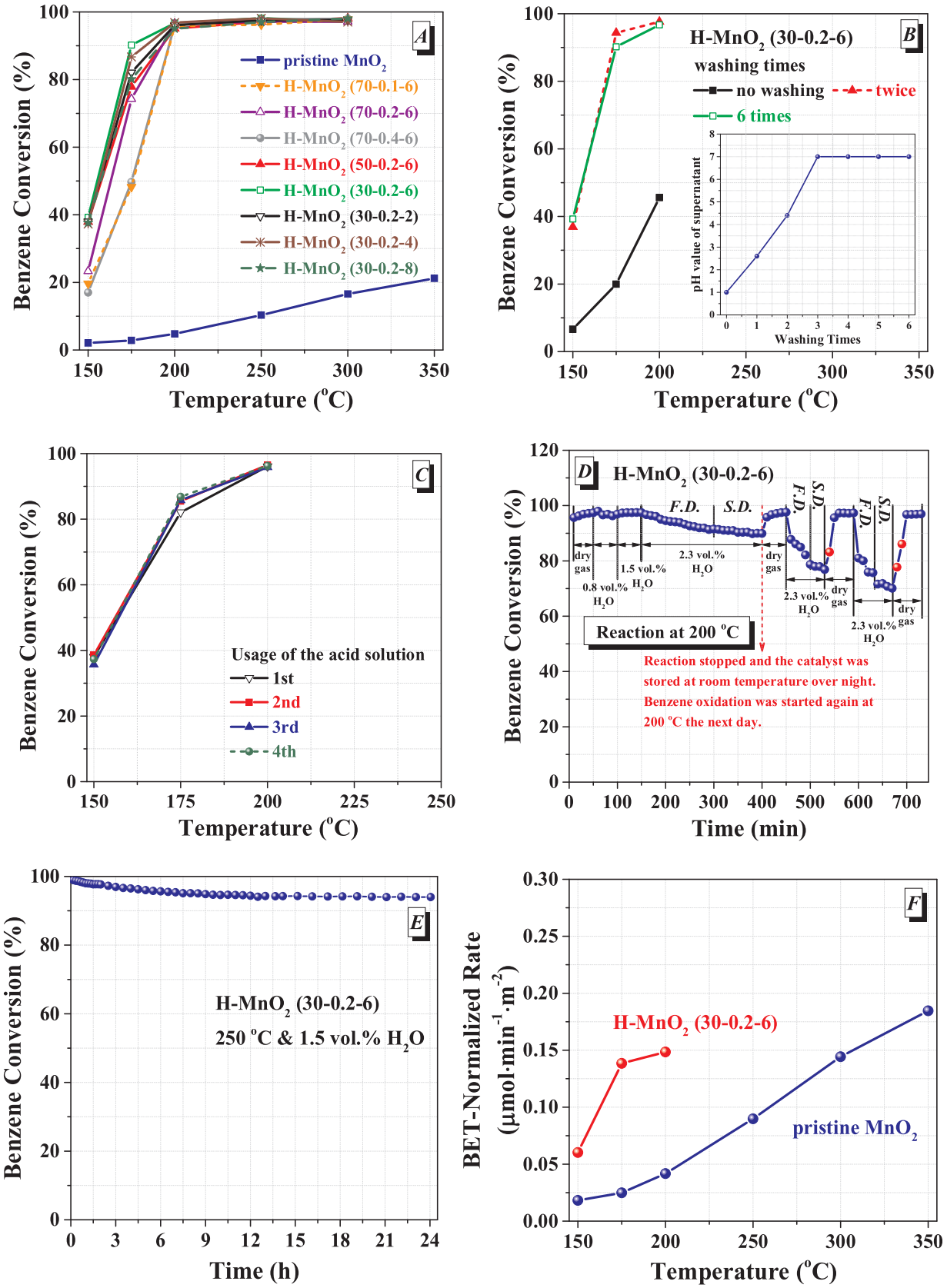


**Fig. 1.** **(A)** Temperature profiles of benzene conversion over the pristine and acid-treated $MnO_2$, **(B)** Effect of washing times on benzene oxidation over the H-$MnO_2$ (30-0.2-6) catalyst, **(C)** Comparison of benzene oxidation over the samples prepared by the recycled acid solutions, **(D)** Effect of humidity on benzene oxidation over the H-$MnO_2$ (30-0.2-6) catalyst at 200 °C, **(E)** Durability of the H-$MnO_2$ (30-0.2-6) catalyst for long-term reaction at 250 °C under 1.5 vol.% $H_2O$ and **(F)** BET-normalized reaction rates of the pristine $MnO_2$ and H-$MnO_2$ (30-0.2-6). Inset in (B) shows the changes of the pH value of supernatant with washing times. Benzene oxidation conditions: ~0.1 g of catalyst, 200 mL·min$^{-1}$ of synthetic air with 300–400 ppm of benzene.

$CO_2$-TPD was used to measure the interaction of benzene oxidation product with catalyst surface. The conditions of $CO_2$-TPD were similar to those of $O_2$-TPD except that 5 vol.% $O_2$/He was changed to pure $CO_2$ gas during adsorption stage.

## 3. Results and discussion

### 3.1. Activity tests

#### 3.1.1. The optimal treatment conditions of birnessite $MnO_2$

Catalytic benzene oxidation over the pristine $MnO_2$ or H-$MnO_2$ obtained via different treatment conditions is comparatively shown in Fig. 1A to screen the optimal parameters of acid treatment, which clearly indicates that $HNO_3$ treatment remarkably enhanced benzene oxidation activity of birnessite $MnO_2$. When reaction temperature was lower than 200 °C, the pristine $MnO_2$ was almost inactive toward benzene oxidation with only 5% of benzene degraded at 200 °C and ~20% at an even higher temperature of 350 °C. After the pristine $MnO_2$ was treated with $HNO_3$, almost complete removal of benzene could be achieved at 200 °C with ~97% of removal efficiency regardless of the acid treatment conditions.

Moreover, it is also proposed from Fig. 1A that a proper combination of $HNO_3$ aqueous concentration, treatment temperature and treatment period is essential for the high activity of the H-$MnO_2$ catalysts. As to the $HNO_3$ aqueous concentration, it had an optimal value, neither too low nor too high. Treatment in 0.2 M of $HNO_3$ solution resulted in relatively better benzene oxidation performance, as seen from the comparison among H-$MnO_2$ (70-0.1-6), H-$MnO_2$ (70-0.2-6) and H-$MnO_2$ (70-0.4-6). Acid treatment at high temperature was not conductive to benzene oxidation since the benzene oxidation activity decreased in the sequence of H-$MnO_2$ (30-0.2-6) > H-$MnO_2$ (50-0.2-6) > H-$MnO_2$ (70-0.2-6). Four acid treatment periods (2 h, 4 h, 6 h and 8 h) were evaluated in this study and the changes of benzene conversion with the period of acid treatment exhibited volcano shape with 6 h being the optimal treatment time when the $HNO_3$ concentration and treatment temperature were fixed at 0.2 M and 30 °C, respectively. In particular, when the pristine $MnO_2$ was treated in 0.2 M of $HNO_3$ aqueous solution at 30 °C for 6 h, the as-obtained H-$MnO_2$ (30-0.2-6) catalyst possessed the highest activity, exhibiting ~40%, ~90% and ~97% of removal efficiency for 395 ppm of benzene under 120 $L\,g^{-1}\,h^{-1}$ of space velocity at 150 °C, 175 °C and 200 °C, respectively. The $CO_2$ yield (%) was defined as the concentration ratio of formed $CO_2$ to the inlet benzene. The $CO_2$ yields of the catalysts at the reaction temperature of 175 °C are shown in Fig. S1. There was no $CO_2$ formed over the pristine $MnO_2$, and except the H-$MnO_2$ (30-0.2-6), the $CO_2$ yields of the other acid-treated samples were less than the corresponding benzene conversions to different extents, indicating the formation of oxidation by-products over these samples. The $CO_2$ yield of the H-$MnO_2$ (30-0.2-6) was almost the same as the corresponding benzene conversion (Fig. 1A), demonstrating its good mineralization rate. Therefore, the H-$MnO_2$ (30-0.2-6) catalyst was used for further study in the following sections. In our previous study [28], the $T_{50}$ and $T_{90}$ (corresponding to the respective reaction temperatures at which 50% and 90% of benzene conversions could be obtained) of the prepared Cu-modified birnessite $MnO_2$ were 193 °C and 240 °C, respectively, which were superior over the reported birnessite samples and were comparable to the noble metal catalysts in literature. As shown in Fig. 1A, the $T_{50}$ and $T_{90}$ of the H-$MnO_2$ (30-0.2-6) were 155 °C and 175 °C, respectively, obviously lower than those of the Cu-modified birnessite $MnO_2$, thereby paving road for the preparation of active benzene decomposition catalysts with potential for real-world application in the future.

#### 3.1.2. Effect of washing times

Although the water washing process is critical during catalyst preparation, it consumes a large amount of water in mass production of solid materials. In view of the lack of fresh water resources in China, the effect of washing times after acid treatment and centrifugal separation on benzene oxidation activity of the H-$MnO_2$ (30-0.2-6) was examined in this study. Dependence of benzene conversion on washing times is plotted in Fig. 1B. The pH value of the supernatant after each centrifugal separation increased with washing time and reached neutral after washing three times, as seen from the inset. Water washing is a compulsory step to render a high catalytic activity, testified by the greatly enhanced benzene conversion over the washed samples with respect to no washing, while there was no significant difference between washing twice and six times. As reported by Thevenet et al. [32], the existence of nitrate species ($NO_3^-$) over the catalyst surface would block the active sites for acetaldehyde adsorption; besides, Lin et al. [33] found that N-containing intermediates, including nitrate, were accumulated on the catalyst surface during ozonation of NO, resulting in the occupation of the catalytically active sites. Therefore, in this study, the inferior activity of the catalyst without water washing in comparison with the thoroughly washed sample is likely due to the poisoning effect of $NO_3^-$, which was deposited over the acid-treated surface during $HNO_3$ treatment. Thorough washing until the eluate becomes neutral is more easily controlled and more conducive to the reproducible production of the catalyst. Thus, washing six times was selected throughout this paper.

#### 3.1.3. Reusability of the acid solution for GREEN process

As seen from the inset in Fig. 1B, the supernatant after the first centrifugal separation had a pH value of ~1.0, which was not allowed to be discharged directly without any treatment. Therefore, from the viewpoint of Green chemistry and recycling, it is important to investigate the reusability of the acid solution for multiple productions of catalysts. As shown in Fig. 1C, the activities of the H-$MnO_2$ samples prepared by the recycled acid solutions showed no decrease with respect to the sample prepared by the fresh acid solution, highlighting the feasibility of reusing the acid solution over times, and the synthetic strategy of birnessite material efficient for benzene oxidation by $HNO_3$ treatment thereby can be considered environmentally friendly.

#### 3.1.4. Effects of humidity in feed gas and temperature fluctuation

As seen from the discussion above, the H-$MnO_2$ (30-0.2-6) sample is important for low-temperature removal of air benzene. However, the unavoidable moisture is not conductive to the desired reaction [34] and the water-resistant materials are very desirable. Therefore, the effect of humidity in feed gas on benzene oxidation over the H-$MnO_2$ (30-0.2-6) at 200 °C was then investigated. As shown in Fig. 1D, under the 0.8 vol.% and 1.5 vol.% of $H_2O$ the catalyst did not show reduced activity with respect to the dry-gas reaction, all the three cases keeping ~97% of benzene conversion during the entire test. However, further increasing humidity to 2.3 vol.% resulted in gradual deactivation of the catalyst, and the benzene conversion was finally maintained around 90% after 4 h reaction. After the above four-stage reactions (50 min each for dry reaction, 0.8 vol.% and 1.5 vol.% of $H_2O$, and then 4 h for 2.3 vol.% of $H_2O$), the feed gas was stopped and the catalyst was cooled down and stored at room temperature overnight. When benzene oxidation was started again at 200 °C in dry gas the next day with the formerly used catalyst, benzene conversion still could be stably kept around 97% as before, suggesting that the H-$MnO_2$ (30-0.2-6) catalyst could be repeatedly used after heating and cooling processes, which are often encountered during practical applications. Thereafter, the benzene removal rate was evaluated at alternative dry and humid conditions. When the catalyst was subject to humid air with 2.3 vol.% of $H_2O$ again, much faster and severer deactivation was observed with benzene conversion dropping from ~97% to ~77% in 80 min. Whereas, benzene conversion could be recovered to ~97% if the water vapor was cut off, but the recovery rate was slower than the latest cycle, as indicated by the number of the red data point, 10 min each. Most importantly, once the $H_2O$ content returned to 2.3 vol.%, benzene conversion was quickly reduced to the level worse than the latest cycle, indicating that the

effect of water vapor was accumulated and did not disappear after treated in dry gas flow. As far as we know, there are different water-induced deactivation mechanisms for catalytic VOCs oxidation reported in literature. Chen et al. [35] reported that the oxidation of toluene followed a series of steps (toluene→intermediate→$CO_2$), and the intermediate→$CO_2$ step consumed more oxygen. Therefore, the decreasing oxygen concentration by introducing water was more negative to the transformation of intermediates to $CO_2$, resulting in the accumulation of oxidation byproducts over the catalyst surface and finally catalyst deactivation. On the other hand, the activity inhibition by water vapor is also likely to be the result of the competitive adsorption of water with benzene as well as oxygen molecules [34], which decreased the number of the catalytically active sites available for benzene oxidation. From Fig. 1D, it can be seen that when 2.3 vol.% of humidity was introduced into the feed gas, fast deactivation (*F.D.*) followed by slow deactivation (*S.D.*) was observed. Based on the discussion above, we think that the initial fast deactivation is due to the occupation of catalytically active sites by water molecules and the later slow deactivation is resulted from the gradual accumulation of surface intermediates.

#### 3.1.5. Long-term stability in humid stream with 1.5 vol.% $H_2O$

The stability of the H-$MnO_2$ (30-0.2-6) catalyst for long-term oxidation of gaseous benzene was further tested. As shown in Fig. 1E, only a slight deactivation was observed in the first few hours and the H-$MnO_2$ (30-0.2-6) catalyst showed excellent stability during 24-h continuous test, keeping a stable removal efficiency of ~94% for 318 ppm of benzene under a high space velocity of 120 $L{\cdot}g^{-1}\,h^{-1}$ and 1.5 vol.% of $H_2O$ at 250 °C.

Notably, as shown in Table 1, except the two samples tested under the very high humidities (3.6 vol.% and 7.2 vol.%), which are too high for our activity evaluation system to realize, the excellent water-resistant property of the H-$MnO_2$ (30-0.2-6) is better than those of the reported materials, even though the space velocity (60 $L{\cdot}g^{-1}\,h^{-1}$) adopted in these cases was only half the value adopted in this study (120 $L{\cdot}g^{-1}\,h^{-1}$). Thus, the H-$MnO_2$ (30-0.2-6) catalyst used in this study is a potential candidate for the remediation of benzene pollution from real air.

In the next section, the properties of the H-$MnO_2$ (30-0.2-6) were comparatively studied with the pristine $MnO_2$ through various characterizations and deliberately designed experiments to elucidate the underlying mechanism for the promoting effect of acid treatment on benzene oxidation.

### 3.2. Characterization studies

#### 3.2.1. Crystal structure, morphological changes and surface elements

XRD patterns of the pristine $MnO_2$ and H-$MnO_2$ (30-0.2-6) are displayed in Fig. 2A. The diffraction peaks around 12.0° {001}, 25.2° {002}, 37.6° {-111}, 42.3° {-112} and 66.5° {005} were observed over the pristine sample, which are well indexed to the standard information of birnessite $MnO_2$ (JCPDS 80-1098) without detectable impurity peaks, testifying the formation of layered structure but with poor crystallinity. It is also found that no phase changes occurred after acid treatment, although the relative intensities are slightly different. This could be ascribed to the partial destabilization of the layered structure from the leaching of $K^+$ cations [40] by $H^+$ ions in $HNO_3$, which will be discussed in the following EDS mapping and XPS measurements. Even after heat treatment at 200 °C and 300 °C for 3 h, the poor birnessite crystal structure was still retained, as shown in Fig. S2, indicating the good thermal stability of the catalysts. Thus, the influence of the changes of crystal structure on the catalytic performance in Fig. 1A could be excluded.

Morphological changes of the birnessite $MnO_2$ before and after acid treatment were studied by SEM. As shown in Fig. 2(B-1), the pristine $MnO_2$ (left image) was mainly present in compact layered structure, which is in accordance with the XRD result (Fig. 1A); however, this kind of compact morphology was significantly alleviated after acid treatment (right image), thus leading to the dramatic increase in $S_{BET}$ (from 40 $m^2\,g^{-1}$ to 230 $m^2\,g^{-1}$), which played an important role in enhancing the contact efficiency between gaseous reactants and catalyst surface. Some of the layered structure was transformed into rods over the H-$MnO_2$ (30-0.2-6) catalyst, as pointed by the green arrows. $K^+$ usually acts as layer adhesive, so the loss of $K^+$ by $H^+$ leaching, as evidenced by the following EDS mapping and K 2p XPS spectra, would cause destabilization of the layered structure [23,41], resulting in the smaller particle size. Considering the marked difference in BET surface areas of the pristine and acid-treated samples, the activities obtained from Fig. 1A could not reflect the intrinsic activities. Therefore, the normalized specific activities of the pristine $MnO_2$ and H-$MnO_2$ (30-0.2-6) to their BET surface areas were calculated since the BET surface area has been widely employed for metal oxide catalyst comparison [42]. As

**Table 1**
Summary of the reported data on catalytic oxidation of gaseous benzene in humid stream.

| Sample | Preparation | Test conditions | *X* (*T*) [a] | Ref. |
|---|---|---|---|---|
| Mixture of $Mn_2O_3$ and $Mn_3O_4$ | Reaction between $(NH_4)_2C_2O_4$ and $Mn^{2+}$ followed by 450 °C calcination | 500 ppm $C_6H_6$/air<br>1.56 vol.% $H_2O$<br>60 $L{\cdot}g^{-1}{\cdot}h^{-1}$ | 47% (200 °C)<br>97% (250 °C) | [34] |
| $Cu_{0.5}Co_{2.5}Al$ | Co-precipitation of $Cu^{2+}$, $Co^{2+}$ and $Al^{3+}$ with $Na_2CO_3$ followed by 400 °C calcination | 500 ppm $C_6H_6$/air<br>1.5 vol.% $H_2O$<br>60 $L{\cdot}g^{-1}{\cdot}h^{-1}$ | 92% (320 °C) | [36] |
| $Cu_{0.6}Mn$ | Nanocasting synthesis with mole ratio of Cu/Mn = 0.6 | 500 ppm $C_6H_6$/air<br>1.5 vol.% $H_2O$<br>60 $L{\cdot}g^{-1}{\cdot}h^{-1}$ | 90% (260 °C) | [37] |
| $CoMn_2AlO$-550 | Co-precipitation of $Co^{2+}$, $Mn^{2+}$ and $Al^{3+}$ with $NH_4OH$ followed by hydrothermal treatment and 550 °C calcination | 100 ppm $C_6H_6$/air<br>7.2 vol.% $H_2O$ [b]<br>60 $L{\cdot}g^{-1}{\cdot}h^{-1}$ | 40% (190 °C)<br>100% (230 °C) | [38] |
| $Co^{II}Co^{III}$ layered double hydroxide | Mixed stirring $Co(NO_3)_2$ with ammoniacal nitrogen followed by 400 °C calcination | 100 ppm $C_6H_6$/air<br>3.6 vol.% $H_2O$ [b]<br>60 $L{\cdot}g^{-1}{\cdot}h^{-1}$ | 98% (230 °C) | [39] |
| Cu modified birnessite | Redox between $KMnO_4$ and $Mn^{2+}$ followed by $Cu^{2+}$ exchange | 314 ppm $C_6H_6$/air<br>1.5 vol.% $H_2O$<br>120 $L{\cdot}g^{-1}{\cdot}h^{-1}$ | 90% (300 °C) | [28] |
| H-$MnO_2$ | Redox between $KMnO_4$ and $CH_3OH$ solution followed by $HNO_3$ treatment | 318 ppm $C_6H_6$/air<br>1.5 vol.% $H_2O$<br>120 $L{\cdot}g^{-1}{\cdot}h^{-1}$ | 57% (200 °C)<br>94% (250 °C) | This work |

[a] *X* (*T*) represents benzene conversion (*X*) at a specific reaction temperature (*T*).
[b] These two humidities are too high for our activity evaluation system to realize at the time of submission.

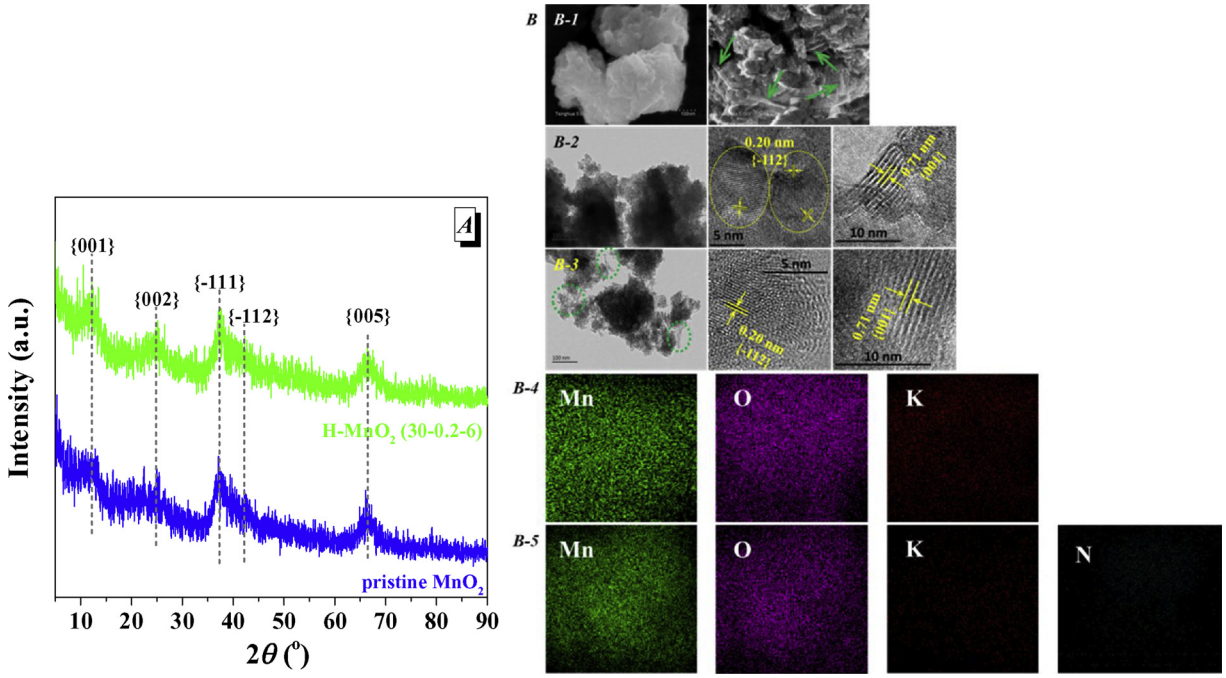


**Fig. 2. (A)** XRD patterns and **(B)** SEM & (HR)TEM images and EDS elemental maps of the catalysts. The left image in B-1 and Images B-2 & B-4 represent the pristine $MnO_2$; the right image in B-1 and Images B-3 & B-5 represent the H-$MnO_2$ (30-0.2-6).

exhibited in Fig. 1F, the H-$MnO_2$ (30-0.2-6) outperformed the pristine $MnO_2$ with much higher specific reaction rates, demonstrating the excellent intrinsic reactivity of the reaction sites over the H-$MnO_2$ (30-0.2-6).

The (HR)TEM images of the pristine $MnO_2$ and H-$MnO_2$ (30-0.2-6) are exhibited in Fig. 2(B-2) and (B-3), respectively. The layered structure was also observed by TEM over both samples, and rods were detected over the H-$MnO_2$ (30-0.2-6) circled by green dashes, which agrees well with the above SEM observations. In addition, it is found that acid treatment had little effect on the exposed facets and both samples exposed the typical crystal planes of birnessite $MnO_2$, which was confirmed in many areas throughout the sample (not all the HRTEM photos were given in this study). However, the sharpness of the lattice fringes before and after acid treatment was very different, and the lattice fringes of the H-$MnO_2$ (30-0.2-6) became blurred compared with the pristine $MnO_2$, as manifested by the comparative observation of the {-112} and {001} planes of the two samples. This result suggests that the formation of crystal defect by acid treatment caused distortion to the ordered lattice structure of the birnessite $MnO_2$. To investigate the composition distributions, the EDS mapping images were taken, which show that Mn and O were evenly distributed over both samples (Fig. 2(B-4) and (B-5) before and after acid treatment, respectively). The K signal of the H-$MnO_2$ (30-0.2-6) was much weaker than that of the pristine $MnO_2$ as a result of $K^+$ replacement by $H^+$ exchange. The existence of $H^+$ in the acid-treated birnessite $MnO_2$ was supported by the $H^1$-NMR characterization in our previous study [23]. No residual N element was detected over the H-$MnO_2$ (30-0.2-6) probably due to the thorough washing after acid treatment.

The effects of crystal structure and exposed facet on benzene oxidation activity thereby could be ruled out as evidenced by the above XRD and HRTEM results. Considering that catalytic activity is highly related to the surface electronic structure, the role of the oxidation state of surface elements in determining the benzene oxidation performance was then investigated by XPS, with the results depicted in Fig. 3. The empirical relationship between the average oxidation state (AOS) of surface Mn atoms and the Mn 3 s multiplet energy ($\Delta E$) is useful and reliable to estimate the chemical valence of Mn element since the binding energies of different Mn valences in Mn 2p spectra are close to each other [43], thus making it difficult to fulfill objective and definite deconvolutions. Substitute the values of $\Delta Es$ in Fig. 3A into the formula of AOS = 9.27 - 1.18 × $\Delta E$ [44], and the AOSs of Mn were worked out. As listed in Table 2, the AOS of Mn over the H-$MnO_2$ (30-0.2-6) surface was ˜3.5, lower than that of the pristine $MnO_2$ by 0.2. The lower Mn valence resulted from acid treatment was also confirmed by the Mn 2p results, shown in Fig. 3B. Two peaks, centered at ˜653.0 eV and ˜641.0 eV, were observed over both samples, corresponding to the Mn $2p_{1/2}$ and Mn $2p_{3/2}$, respectively [45]. Notably, the Mn 2p peaks of the H-$MnO_2$ (30-0.2-6) shifted to lower binding energies compared with those of the pristine $MnO_2$, proving the increased surface electron density after acid treatment. As a result, the valence of the surface Mn decreased over the acid-treated sample. For charge balance, the reduced positive charges thereby will be neutralized by less negatively charged species, *e.g.*, $O^{2-}$, which will induce the formation of oxygen vacancies. Therefore, the H-$MnO_2$ (30-0.2-6) possessed more oxygen vacancies than the pristine sample. Multiple O 1s peaks were observed for both samples (Fig. 3C), indicating the existence of surface oxygen species having varied chemical environments. According to literature [46], the O 1s peaks from low to high binding energies could be assigned to the oxygen species from lattice oxygen ($O_{latt}$) and surface adsorbed oxygen ($O_{ads}$). Also as shown in Table 2, the H-$MnO_2$ (30-0.2-6) had higher surface $O_{ads}/O_{total}$ ratio ( = 0.45) with respect to the pristine $MnO_2$ ( = 0.23), testifying the generation of more surface active oxygen sites by acid treatment. What is more, the surface adsorbed oxygen content can reflect the amount of surface oxygen vacancies on the basis of the concept that oxygen molecules are usually adsorbed on the oxygen vacancy sites over metal oxides [47]. Apparently, the higher $O_{ads}/O_{total}$ ratio of the H-$MnO_2$ (30-0.2-6) signifies its larger amount of oxygen vacancies, consistent with the Mn 3 s data that acid treatment of birnessite $MnO_2$ contributed to the formation of oxygen vacancies. The K 2p spectra of the catalysts before and after acid treatment are displayed in Fig. 3D. The K signal was dramatically weakened over the H-$MnO_2$ (30-0.2-6), meaning the loss of $K^+$ ions due to the leaching effect of $H^+$ exchange during acid treatment. This result agrees well with the elemental distributions in Fig. 2B.

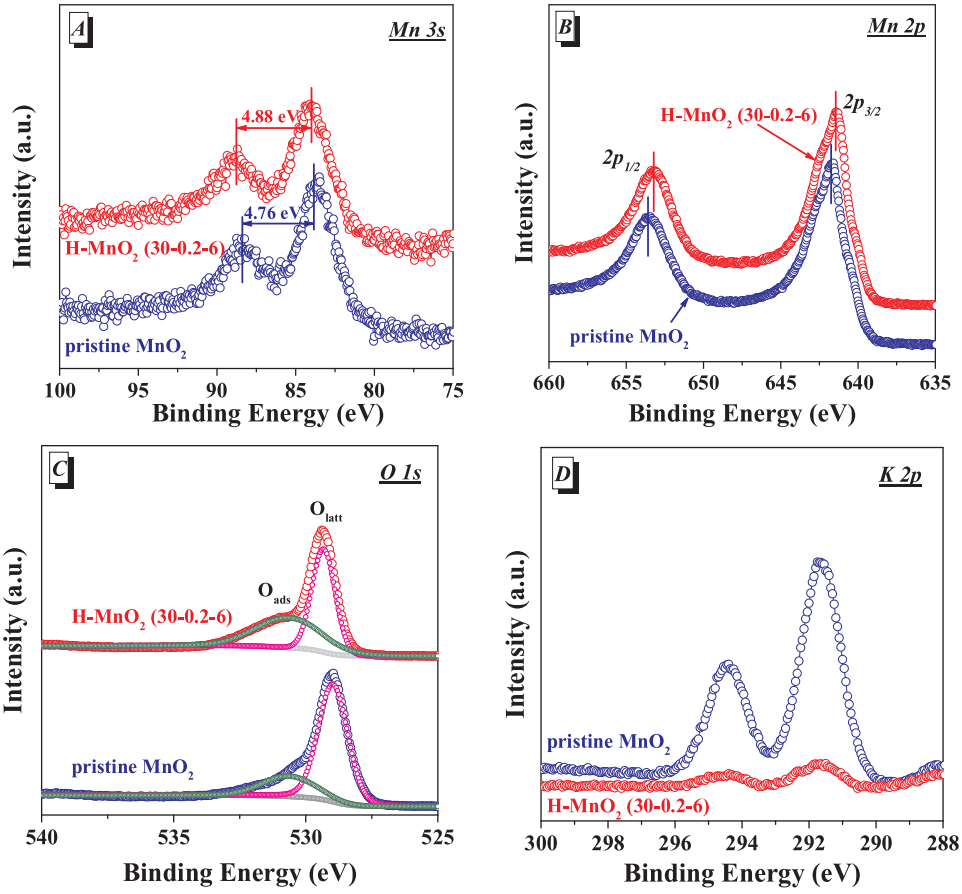


**Fig. 3.** XPS spectra of the catalysts.

**Table 2**
Summary of the XPS results.

| Sample | AOS of Mn | $O_{ads}$ / $O_{total}$ |
|---|---|---|
| pristine $MnO_2$ | 3.7 | 0.23 |
| H-$MnO_2$ (30-0.2-6) | 3.5 | 0.45 |

### 3.2.2. Redox behavior and surface acidity

$H_2$-TPR is a good method to evaluate the redox properties of solid materials, which can be correlated with their catalytic performances for oxidation reactions [48]. Chen et al. [49,50] reported that the good reducibility of the metal oxide catalysts was conducive to the improved performance for toluene oxidation. The $H_2$-TPR results of the pristine $MnO_2$ and H-$MnO_2$ (30-0.2-6) are shown in Fig. 4A. For the pristine $MnO_2$, the reduction mainly occurred from 300 °C to 400 °C with a small reduction peak around 250 °C, denoted as $O_\beta$ and $O_\alpha$, respectively. According to the Mn 3 s XPS results, the Mn AOS of the pristine $MnO_2$ was about 3.7 (Table 2), suggesting that Mn mainly existed as mixture of $Mn^{3+}$ and $Mn^{4+}$. Thus, at a first glance, these two peaks belong to the continuous reductions of manganese oxide, which, however, is not the case. Based on the deconvolution and integration results, the peak area ratio of $O_\alpha$ to $O_\beta$ was about 4:13, which is quite different from the theoretical value of 7:13 obtained from the consecutive reductions of $MnO_2$ to $Mn_2O_3$ to MnO and the fact that the atomic ratio of $Mn^{3+}$ to $Mn^{4+}$ over the pristine $MnO_2$ was 3:7 according to its Mn AOS. In addition, the peak area ratio of $O_\alpha$ to ($O_\alpha$ + $O_\beta$) was ˜0.24, very close to the content of surface adsorbed oxygen over the pristine $MnO_2$ ( = 0.23, Table 2). It is thereby reasonable to deduce that the $O_\alpha$ and $O_\beta$ peaks in the $H_2$-TPR profile of the pristine $MnO_2$ are assigned to the respective reductions of the oxygen species from surface adsorbed oxygen and $MnO_x$ lattice. After acid treatment, significant changes happened to the redox behavior of the birnessite $MnO_2$, mainly in the low-temperature range (< 300 °C). In addition to the $H_2$ consumption peak near 250 °C ($O_\alpha$), another strong and sharp reduction peak was detected at 293 °C. The peak area ratio of $O_\alpha$ to the total oxygen species was ˜0.41, almost the same as the content of surface adsorbed oxygen over the H-$MnO_2$ (30-0.2-6) ( = 0.45, Table 2), further confirming that the $O_\alpha$ peak belongs to the reduction of surface adsorbed oxygen. The starting reduction temperature of $O_\alpha$ was 113 °C over the H-$MnO_2$ (30-0.2-6), much lower than that over the pristine $MnO_2$ ( = 136 °C), as seen in the inset, demonstrating that acid treatment increased the activity of surface adsorbed oxygen, thus lowering the reduction temperature. Additionally, the 293 °C and 360 °C peaks over the H-$MnO_2$ (30-0.2-6) are tentatively attributed to the consecutive reductions of the $MnO_x$ lattice oxygen ($O_\beta$). However, the peak area ratio of these two peaks was calculated to be about 1:1, which is larger than theoretical value of 1:3 based on the consecutive reductions of $MnO_2$ to $Mn_2O_3$ to MnO and the fact that the atomic ratio of $Mn^{3+}$ to $Mn^{4+}$ was 1:1 according to the Mn AOS of 3.5. The plausible explanation might be that the lattice oxygen became more facile and reducible because of acid treatment, thus resulting in the early reduction.

The changes of surface acidity of the birnessite $MnO_2$ after acid treatment were assessed by pyridine adsorbed IR spectroscopy to determine the nature and obtain the amounts of the acid sites between Lewis-acid sites (L-sites) and Brønsted-acid sites (B-sites). As reported by Wu et al. [51], the L-sites act as the core active sites for the cleavage of the C—C bands in the benzene ring, which is important to the complete oxidation of benzene. The pyridine-IR spectra of the pristine $MnO_2$ and H-$MnO_2$ (30-0.2-6) at 40 °C, 100 °C and 200 °C are shown in Fig. 4B. According to the literature [51], the peak assignments were as follows: the peak at 1540 $cm^{-1}$ is attributed to pyridine adsorbed on B-sites, and bands at 1610 $cm^{-1}$ and 1450 $cm^{-1}$ are due to pyridine

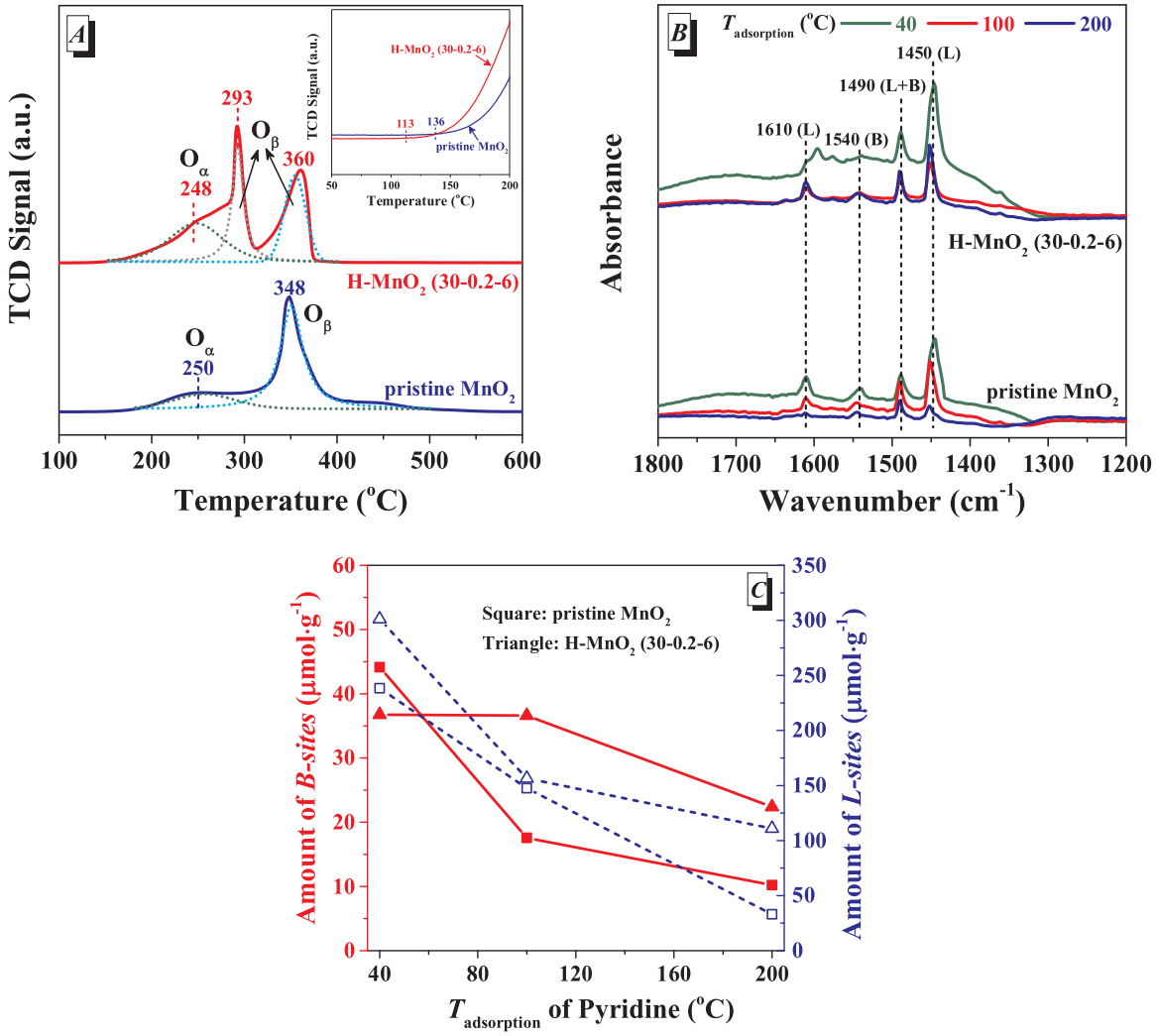


**Fig. 4. (A)** $H_2$-TPR profiles of the catalysts, **(B)** Pyridine-IR spectra of the pristine $MnO_2$ and H-$MnO_2$ (30-0.2-6) at 40 °C (——), 100 °C (——) and 200 °C (——), and **(C)** Amounts of the Lewis-acid sites and Brønsted-acid sites over these two samples plotted against the adsorption temperature of pyridine. $H_2$-TPR conditions: ~0.05 g of catalyst, 50 mL·min$^{-1}$ of 5 vol.% $H_2$/Ar, 10 °C·min$^{-1}$.

adsorbed on L-sites; the band at 1490 cm$^{-1}$ is resulted from pyridine adsorbed on both L-sites and B-sites. The peak intensities decreased as the catalyst was heated to higher temperatures due to the desorption of pyridine adsorbed on weak acid sites, but the decreasing extent was quite different between the pristine and acid-treated samples. In this study, the adsorbed pyridine at 200 °C was used to assess the amount of strong acid sites, and the adsorbed pyridine at 40 °C was used to calculate the total amount of acid sites. For clarity, the amounts of the L-sites and B-sites over these two samples are plotted against the adsorption temperature of pyridine in Fig. 4C, which manifests that the L-sites dominated over the B-sites for both samples at all three adsorption temperatures and the acid-treated surface could provide more acid sites, including the strong B- and L-sites, than the pristine $MnO_2$. The larger amount of acid sites and the stronger acidity of the H-$MnO_2$ (30-0.2-6) might also facilitate benzene oxidation [51,52].

*3.2.3. Interaction of reactants and products with catalyst and activation of reactant molecules*

*3.2.3.1. Interaction and activation of benzene with catalysts*. Benzene adsorption and then desorption in $N_2$ ($C_6H_6$-TPD) was used to study the interaction and activation of benzene molecules with catalyst surface. As shown in Fig. 5A, at benzene adsorption stage, the outlet benzene concentration did not change too much when the benzene feed gas flowed through the pristine $MnO_2$ whereas it decreased to a much lower value over the H-$MnO_2$ (30-0.2-6), substantiating the higher adsorption capacity of benzene induced by acid treatment. During $N_2$ purging (benzene was cut off), which was used to desorb the physiosorbed benzene, for the pristine $MnO_2$, the outlet benzene concentration decreased fast to nearly 15 ppm in ~1 h, which, however, dropped much more slowly over the H-$MnO_2$ (30-0.2-6), and about 40 ppm of benzene could still be detected even after ~3-h purging. When the catalyst covered with benzene was heated with a rate of 10 °C·min$^{-1}$ in $N_2$, benzene desorption peaks centered at 90 °C and 100 °C were detected over the pristine $MnO_2$ and H-$MnO_2$ (30-0.2-6), respectively, and more benzene was evolved from the H-$MnO_2$ (30-0.2-6), inferred from its larger desorption peak, corresponding to 12.3 $mmol_{C6H6}{\cdot}g_{cat}^{-1}$ *vs.* 4.9 $mmol_{C6H6}{\cdot}g_{cat}^{-1}$ by integrating the desorption curves. Besides, another benzene evolution peak was observed at a much higher temperature of 330 °C over the H-$MnO_2$ (30-0.2-6), as shown in the inset, which, however, was not found over the pristine sample. Wan and co-authors [53] carried out $C_6H_6$-TPD measurement over the composites of Fe, Mn and Zr, and benzene evolution occurred at an even higher temperature of 570 °C, which is ascribed to the benzene desorption from catalyst surface. Therefore, in this study, the benzene evolution peak at 330 °C can be ascribed to the benzene desorption from catalyst surface, not due to the re-polymerization of the byproducts during benzene decomposition. The larger adsorption capacity of benzene together with the higher desorption temperatures

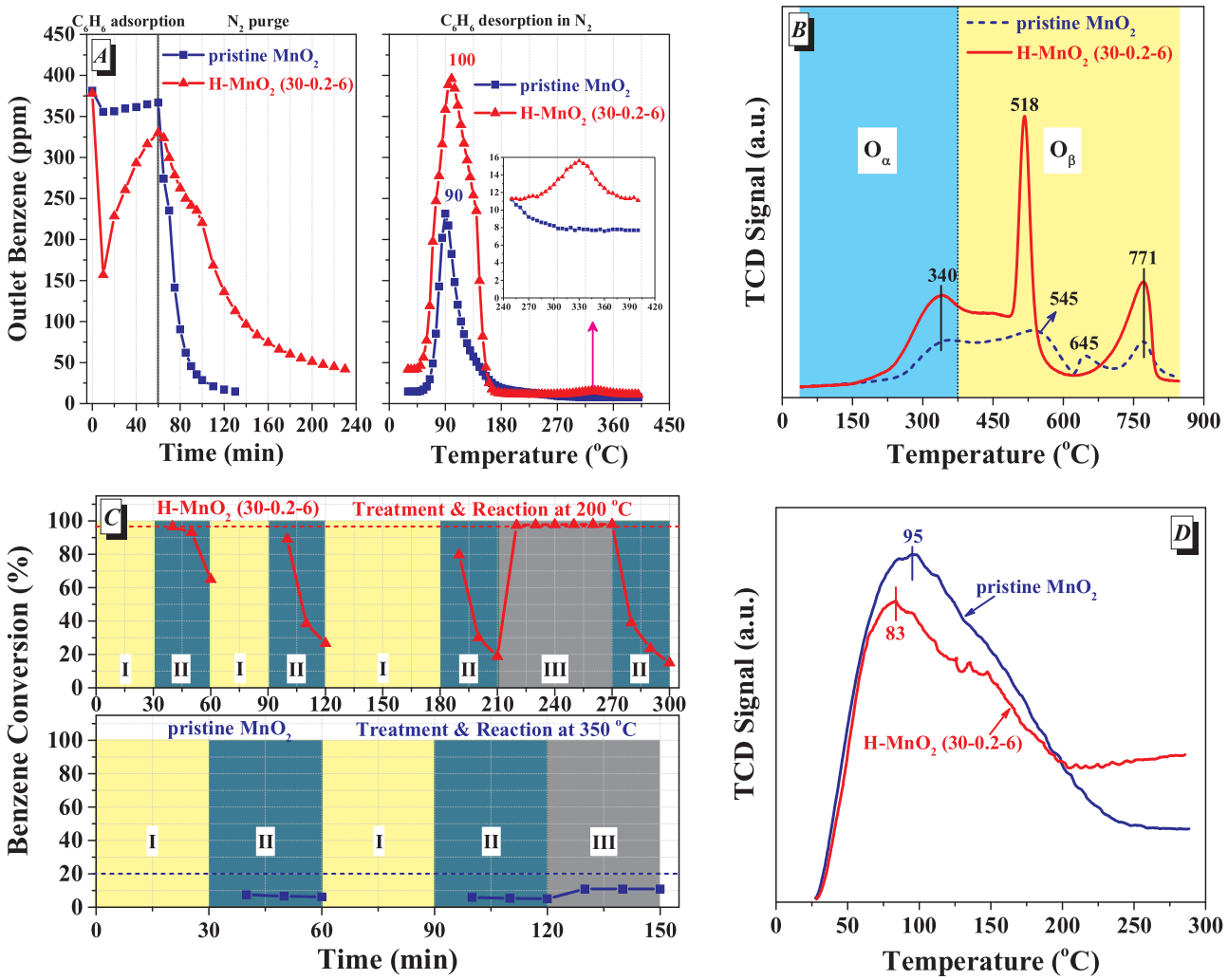


**Fig. 5. (A)** $C_6H_6$-TPD, **(B)** $O_2$-TPD, **(C)** $C_6H_6$-SOR and **(D)** $CO_2$-TPD of the catalysts. For $C_6H_6$-TPD: ~0.1 g of catalyst, 200 mL·min$^{-1}$ of $N_2$ with ~380 ppm of benzene for 1 h adsorption, room temperature; 200 mL·min$^{-1}$ of pure $N_2$ for desorption, 10 °C·min$^{-1}$. For $O_2$-TPD: ~0.05 g of catalyst, 50 mL·min$^{-1}$ of 5 vol.% $O_2$/He for 30-min adsorption, room temperature; 50 mL·min$^{-1}$ of helium for desorption, 10 °C·min$^{-1}$. Reaction conditions for Zone (I), (II) and (III) in (C) are as follows: treatment in 100 mL·min$^{-1}$ of synthetic air; 200 mL·min$^{-1}$ of $N_2$ containing ~380 ppm of benzene; 200 mL·min$^{-1}$ of synthetic air containing ~380 ppm of benzene, and the treatment and reaction temperatures were 350 °C and 200 °C for the pristine $MnO_2$ and H-$MnO_2$ (30-0.2-6), respectively. The conditions of $CO_2$-TPD were similar to those of $O_2$-TPD except that 5 vol.% $O_2$/He was changed to pure $CO_2$ gas during adsorption stage.

of adsorbed benzene over the H-$MnO_2$ (30-0.2-6) might be correlated with its larger amount of acid sites and stronger surface acidity (pyridine IR, Fig. 4B and C) since acid sites play an important role in the adsorption of hydrocarbons [52]. Conclusively, the much stronger affinity of gaseous benzene to the acid-treated surface would probably result in an easier activation of benzene molecules during benzene oxidation reaction.

*3.2.3.2. Interaction and activation of oxygen with catalysts.* Oxygen adsorption and then desorption in helium ($O_2$-TPD) was used to study the interaction and activation of oxygen molecules with catalyst surface, with the results shown in Fig. 5B. According to the literature [54], for both the pristine $MnO_2$ and H-$MnO_2$ (30-0.2-6), their $O_2$-TPD curves could be divided into two parts: the $O_2$ evolved at temperatures below 400 °C and higher than 400 °C are assigned to the release of surface adsorbed oxygen ($O_\alpha$) and lattice oxygen ($O_\beta$), respectively. Although the surface adsorbed oxygen had the same desorption temperature (~340 °C) over both samples, acid treatment evidently increased the amount of surface adsorbed oxygen, judged from the larger desorption peak of $O_\alpha$ over the H-$MnO_2$ (30-0.2-6), which demonstrates that the acid-treated surface provided more sites, *i.e.*, oxygen vacancies, to accommodate oxygen species. This is in accordance with the O 1s XPS (Fig. 3C) and $H_2$-TPR (Fig. 4A) measurements. In terms of lattice oxygen, the peak profiles and peak positions of the acid-treated sample have changed remarkably with respect to the pristine $MnO_2$. For the pristine $MnO_2$, three $O_\beta$ peaks were observed at 545 °C, 645 °C and 771 °C, representing the stepwise desorption of the $MnO_2$ lattice oxygen, *i.e.*, $MnO_2 \rightarrow Mn_2O_3 \rightarrow Mn_3O_4 \rightarrow MnO$ [55]. However, after acid treatment, the 545 °C and 645 °C peaks over the pristine $MnO_2$ were transformed into a strong and sharp peak at a much lower temperature of 518 °C over the H-$MnO_2$ (30-0.2-6), testifying to the generation of more active lattice oxygen by acid treatment. This is also in good accordance with the $H_2$-TPR results (Fig. 4A).

*3.2.3.3. Surface oxidation reaction of benzene ($C_6H_6$-SOR).* There is a definitive consensus in literature that the catalytic oxidation of VOCs proceeds through the Mars-van Krevelen mechanism [56]: the pollutant molecules first adsorb on the catalyst surface, followed by abstracting lattice oxygen species, the pollutant being oxidized and the catalyst being reduced with the formation of oxygen vacancies, which are later replenished by oxygen from gas phase for the next reaction cycle.

Herein, the $C_6H_6$-SOR was specially designed to further clarify the promoting effect of acid treatment on benzene oxidation. $C_6H_6$-SOR was conducted by alternating synthetic air (Zone I) and $C_6H_6/N_2$ (Zone II) through catalyst bed, as displayed in Fig. 5C. Zone I was used to supplement the surface oxygen species and Zone II was used to evaluate the reactivity of the surface oxygen species for benzene oxidation, thus reflecting the activity of surface active sites to activate the oxygen species. The $C_6H_6$-SOR was performed at 350 °C and 200 °C, respectively, over the pristine and acid-treated samples because of the high benzene removal efficiency obtained at the corresponding temperature (Fig. 1A).

For the H-$MnO_2$ (30-0.2-6), during the first "air treatment (Zone I) - benzene oxidation (Zone II)" cycle, benzene could be removed with high efficiency (˜97%), equal to the value achieved by feeding the mixture of benzene and synthetic air into the catalyst (dashed line), in the initial 10 min due to the abundant surface oxygen species; then benzene conversion decreased gradually with reaction time due to the consumption of surface oxygen species; at the end of the first cycle, benzene conversion dropped to 65%. After the catalyst was purged with synthetic air at 200 °C for 30 min, the initial benzene conversion was only recovered to ˜89% in the second cycle and decreased much faster than in the first cycle thereafter. Even if the catalyst was regenerated for 1 h in the third cycle, its benzene conversion still could not be fully recovered, which was lower than that of the second cycle (˜79% *vs.* ˜89%), but the decaying rate of benzene conversion seemed similar to that of the second cycle. According to Föttinger, Rupprechter and their coauthors [57], who performed CO *vs.* $O_2$ switching experiments over $Co_3O_4$, not only surface oxygen might take part in CO oxidation, but also oxygen from the bulk, and the reaction rate with surface oxygen was faster than with the bulk oxygen, which needs to diffuse to the surface to react with CO. Therefore, in this study, it is reasonable to infer that both surface and bulk oxygen participated in benzene oxidation during the first $O_2$ *vs.* benzene switching experiment while only surface oxygen was involved for the following cycles. That is because if only surface oxygen would react during the first cycle, then its benzene conversion should not have dropped less slowly than in the second and third cycles. The above results thus imply that the bulk oxygen was not so easily regenerated as the surface oxygen and the surface oxygen was the main active species for benzene oxidation in this study. When benzene and air simultaneously passed through the catalyst (Zone III), benzene conversion rapidly increased to ˜97% and kept stable for 1 h owing to the continuous replenishment of the surface oxygen by oxygen from gas phase, followed by a rapid reduction once air was cut off again (the last Zone II). Another possibility for the deactivation phenomenon might be due to the accumulation of intermediates or coke deposition. The FT-IR spectrum of the used H-$MnO_2$ (30-0.2-6) after benzene oxidation at 150 °C for 4 h was collected, with the result displayed in Fig. S3, which demonstrates that new peaks due to the oxidation byproducts appeared over the used catalyst in comparison with the fresh sample.

In sharp contrast to the H-$MnO_2$ (30-0.2-6), the activity of the pristine $MnO_2$ to activate surface oxygen species was very poor with less than 10% of benzene being removed at 350 °C (Zone II). Even feeding the mixture of benzene and synthetic air together into the catalyst (Zone III) still could not recover the catalyst (lower than the dashed line). This is because the inert surface oxygen species, which were accumulated over the catalyst surface during the air treatment stage (Zone I), together with the deposition of reaction intermediates (as reflected from the FT-IR spectrum of the used pristine $MnO_2$ after benzene oxidation at 250 °C for 4 h in Fig. S3) occupied the catalytically active sites for reactions. Based on the discussions of $O_2$-TPD and $C_6H_6$-SOR, it can be concluded that compared with the pristine $MnO_2$, the acid-treated surface was much more reactive for the activation of surface oxygen species for benzene oxidation.

*3.2.3.4. The desorption of oxidation products from catalysts.* For catalytic reactions, the desorption of reaction products from catalyst surface is a prerequisite for the regeneration of active sites for the next reaction cycle. Therefore, the easy desorption of products from the catalytically active sites is also important to realize a high and stable activity. As demonstrated by the FT-IR spectra of the used catalysts in Fig. S3, not only $CO_2$ but also other kinds of oxidation products were formed during benzene oxidation. In order to simplify the situation, in this study, the complete oxidation product of benzene, *i.e.*, $CO_2$, was tentatively used as the probe molecule, and the TPD of adsorbed $CO_2$ from the pristine and acid-treated samples was performed to explain the high activity of the acid-treated $MnO_2$ from a new angle of product desorption, with the $CO_2$-TPD curves shown in Fig. 5D. $O_2$ desorption had negligible interference with the $CO_2$-TPD curves because nearly no $O_2$ was desorbed below 200 °C ($O_2$-TPD, Fig. 5B). Both samples exhibited a similar desorption contour of $CO_2$ from 30 °C to 200 °C, but the adsorbed $CO_2$ over the H-$MnO_2$ (30-0.2-6) was more easily desorbed than over the pristine $MnO_2$, as inferred from the lower desorption temperature (83 °C *vs.* 95 °C). Moreover, the pristine $MnO_2$ acted more like a $CO_2$ reservoir since more $CO_2$ was evolved from it, rationalized by its larger desorption peak. Based on the above discussion, the higher activity of the H-$MnO_2$ (30-0.2-6) for benzene oxidation was also related to its weaker interaction with the oxidation product, and the occupied active sites by oxidation products over the acid-treated surface were more easily regenerated.

### 3.3. Discussion on the tremendous effect of acid treatment on benzene oxidation

From a macroscopic point of view, acid treatment decreased the content of interlayer $K^+$ cations of birnessite $MnO_2$ via $H^+$ ion exchange (EDS mapping in Fig. 2B and K 2p XPS in Fig. 3D), which was also accompanied by many changes in microscopic properties. The discussion will be carried out mainly from the following two aspects: benzene activation by surface acid sites and oxygen vacancy promoted activation of surface oxygen.

#### 3.3.1. Benzene activation

The adsorption capacity and binding strength of catalyst surface with pollutant molecules are crucial to the catalytic degradation of pollutants. Wang and coworkers [58] discovered that CO oxidation preferentially occurred over the surface that could provide abundant active sites for CO adsorption, to say, with larger CO adsorption capacity. Weaver et al. [59] investigated the intrinsic reactivity for CO oxidation on single-layer and multilayer PdO {101} grown on Pd {100}, and their DFT calculation results correlated the higher CO oxidation activity of multilayer sample with the stronger binding of CO on multilayer PdO {101}. In this study, benzene adsorption and then desorption in inert gas ($C_6H_6$-TPD, Fig. 5A) was designed to evaluate the capacity and strength of benzene adsorption on the catalysts. The acid-treated $MnO_2$ possessed much larger adsorption capacity for benzene, which was about 2.5 times that of the pristine $MnO_2$ (12.3 $mmol_{C6H6}{\cdot}g_{cat}^{-1}$ *vs.* 4.9 $mmol_{C6H6}{\cdot}g_{cat}^{-1}$). What is more, benzene molecules were more strongly bonded to the acid surface, supported by the higher desorption temperatures of benzene over the H-$MnO_2$ (30-0.2-6) ( = 100 °C and 330 °C) than over the pristine $MnO_2$ ( = 90 °C). As reported by other researchers [52,60], the preferential affinity of the acid-treated surface to benzene molecules might come from its abundant acid sites and strong acidity, especially the L-sites (pyridine-IR, Fig. 4B and C). The L-sites played an important role in the reactions following the Mars-van Krevelen mechanism, as reviewed by Corma and García [61]. The larger amount of benzene adsorption as well as the stronger binding strength of benzene molecules on the H-$MnO_2$ (30-0.2-6) facilitated the activation of benzene for the subsequent thermal oxidation.

#### 3.3.2. Oxygen vacancy promoted activation of surface oxygen

Benzene oxidation on metal oxide catalysts generally goes through a

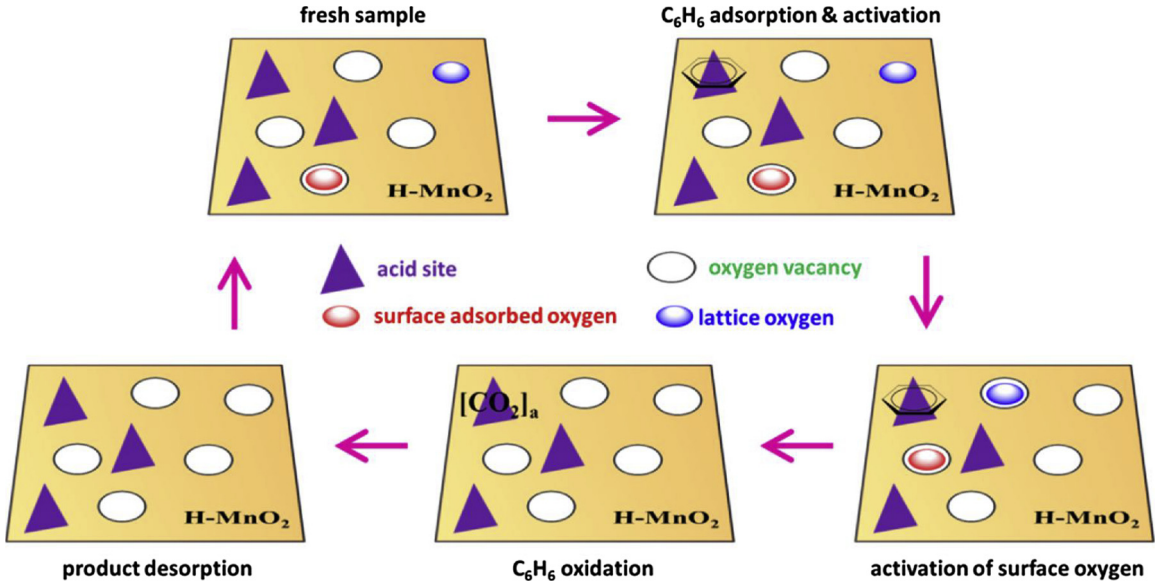


**Fig. 6.** Illustration of benzene oxidation over the H-$MnO_2$ (30-0.2-6).

Mars-van Krevelen mechanism, in which benzene molecules adsorb first on the catalyst surface and are activated, and then oxidized by lattice oxygen. Therefore, besides benzene activation, the activation of surface oxygen species is also crucial to catalytic benzene oxidation. Oxygen vacancy is considered as the active site for the activation of oxygen species. If the number of oxygen atoms is less than what is expected in a perfect crystal, it can be said that oxygen vacancies are formed. Li et al. [25] reported that the presence of oxygen vacancies in $MnO_2$ tremendously improved its catalytic activity for benzene oxidation. Wang et al. [62,63] also pointed out that the defective sites of oxygen on $MnO_2$ were beneficial to formaldehyde oxidation. Acid treatment of birnessite $MnO_2$ increased the number of oxygen vacancy, verified by the Mn 3 s and O 1s XPS measurements (Fig. 3A and C). When it comes to the activity of surface oxygen species, on one hand, acid treatment promoted the mobility of lattice oxygen, as seen from the much lower reduction ($H_2$-TPR, Fig. 4A) and desorption ($O_2$-TPD, Fig. 5B) temperatures of the lattice oxygen over the H-$MnO_2$ (30-0.2-6); on the other hand, the surface adsorbed oxygen over the H-$MnO_2$ (30-0.2-6) also exhibited higher activity than over the pristine $MnO_2$, testified by the lower reduction temperature during $H_2$-TPR measurements. In our previous studies [30,44], it was found that the formation of active surface oxygen species was related to the activity of oxygen vacancies, *i.e.*, the more active the oxygen vacancies are, the more facile and mobile the surface oxygen species will be, from which it can be deduced that compared with the pristine $MnO_2$, the acid-treated sample not only had more oxygen vacancies, but also possessed higher oxygen vacancy activity. The highly active lattice oxygen and surface adsorbed oxygen would react with the activated benzene molecules, which is supported by the $C_6H_6$-SOR experiments (Fig. 5C). Kim and Shim [14] investigated benzene and toluene combustion over a series of manganese oxides and they also correlated the catalytic activity with the oxygen mobility on the catalysts. Moreover, there existed an intrinsic relationship between oxygen vacancy and acid site, and both of them could be correlated with the Mn element. As discussed in the XPS characterization (Fig. 3), lower average oxidation state of Mn implies the formation of more oxygen vacancies, and the amount of oxygen vacancy is related to the $Mn^{3+}$ content. In addition, oxygen vacancy itself is a kind of L-site [64], and oxygen vacancies may be occupied by water and its dissociative species, *i.e.*, surface hydroxyl groups, which usually act as the potential B-sites.

Finally, the easy desorption of oxidation products ($CO_2$-TPD, Fig. 5D) resulted in a fast regeneration of the active sites. At this point, one catalytic cycle over the H-$MnO_2$ (30-0.2-6) is closed. For clarity, the complete reaction cycle for benzene oxidation over the acid-treated surface is illustrated in Fig. 6.

In order to test the universality of the $HNO_3$ treatment method for other $MnO_2$ materials, β-$MnO_2$ (1 × 1 tunnel), α-$MnO_2$ (2 × 2 tunnel) and todorokite $MnO_2$ (3 × 3 tunnel) were prepared, treated by 0.2 M of $HNO_3$ solution at 30 °C for 6 h, and then used in benzene oxidation. Moreover, the commercial Aladdin $MnO_2$ (CAS: 1313-13-9) was also studied. The crystal structures of the as-prepared β-$MnO_2$, α-$MnO_2$ and todorokite $MnO_2$ were confirmed by XRD (Fig. 7A), and the benzene oxidation reactions performed over the pristine and acid-treated samples are comparatively shown in Fig. 7(B–E). Except α-$MnO_2$, acid treatment significantly promoted benzene oxidation over the other three $MnO_2$ samples, especially for the todorokite $MnO_2$, but the acid-treated β-,α- (also the untreated one), todorokite and Aladdin $MnO_2$ were still less active than the acid-treated birnessite $MnO_2$ (H-$MnO_2$ (30-0.2-6)). The different effects of acid treatment and different extents, to which acid treatment could improve the benzene oxidation performance, might be largely dependent on the intrinsic properties of the studied samples. Future studies will be carried out to elucidate this issue.

## 4. Conclusions

In this study, catalytic oxidation of gaseous benzene over birnessite $MnO_2$ was investigated, and the great enhancement by $HNO_3$ treatment on benzene oxidation was clarified by various characterizations and specially designed experiments. The following conclusions could be drawn:

(1) The sample which was treated by 0.2 M of $HNO_3$ aqueous solution at 30 °C for 6 h possessed the best catalytic performance with excellent water resistance, exhibiting a stable removal efficiency of ~94% for 318 ppm of benzene under a high space velocity of 120 $L \cdot g^{-1} h^{-1}$ and 1.5 vol.% $H_2O$ at 250 °C.
(2) The acid treatment method for fabricating high-performance benzene oxidation catalyst is a convenient and green process because the pristine $MnO_2$ was prepared at low temperature and atmospheric pressure, and the acid treatment was carried out at ambient temperature with the $HNO_3$ solution being recycled over times without lowering the catalytic activity.
(3) The increased acid sites and acidity of the acid-treated surface

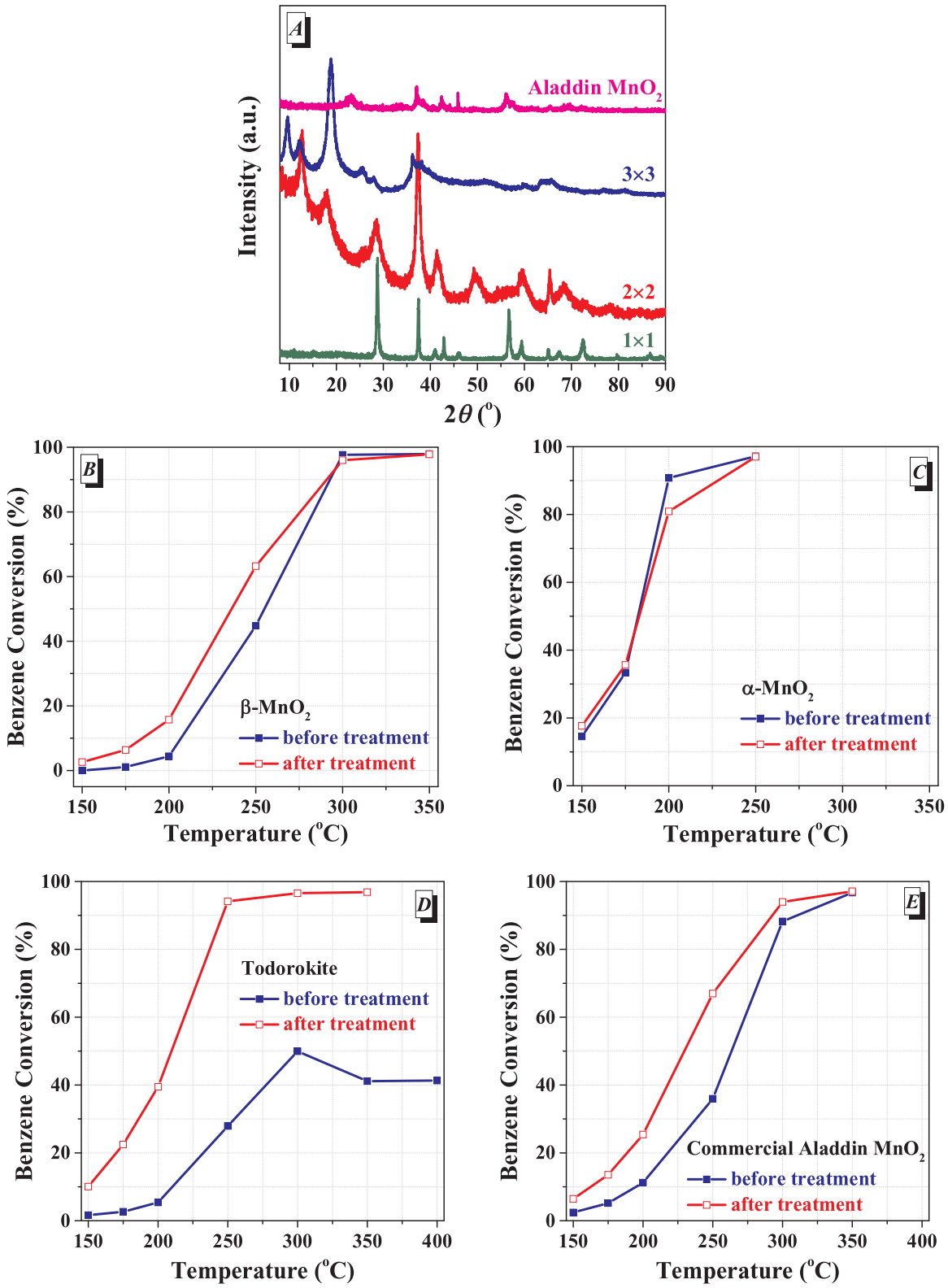


**Fig. 7.** Effects of acid treatment on benzene oxidation were investigated over β-$MnO_2$, α-$MnO_2$, todorokite $MnO_2$ and commercial Aladdin $MnO_2$ to test the universality of the $HNO_3$ treatment method for benzene oxidation: **(A)** XRD patterns of the as-synthesized materials before acid treatment; **(B) to (E)** Benzene conversion *vs.* Reaction temperature. Benzene oxidation conditions were the same as those in Fig. 1A.

(pyridine adsorption IR) promoted the adsorption and activation of gaseous benzene ($C_6H_6$-TPD), and the lattice oxygen and surface adsorbed oxygen became more facile and reactive (surface oxidation reaction of benzene) due to the generated active oxygen vacancies via acid treatment (XPS, $H_2$-TPR and $O_2$-TPD), these two favorable factors together with the easy desorption of reaction products ($CO_2$-TPD) resulting in the excellent performance of the acid-treated sample.

(4) The acid treatment method adopted in this study was universal to other crystal structures of $MnO_2$ except α-$MnO_2$, thereby paving

road for the preparation of active benzene decomposition catalysts with potential for practical application in the future.

## Conflict of interest

There are no conflicts to declare.

## Acknowledgements

This work is supported by National Natural Science Foundation of China (Nos. 21806016, 21677025, 21876022), Dalian University of Technology Fundamental Research Fund (Nos. DUT18RC(3)006, DUT17ZD223) and PetroChina Innovation Foundation (No. 2017D-5007-0609).

All the authors of this article would like to deliver their best wishes to the coming 70th founding anniversary of ***Dalian University of Technology*** since the year of 1949.

## Appendix A. Supplementary data

Supplementary material related to this article can be found, in the online version, at doi:https://doi.org/10.1016/j.apcatb.2019.01.023.

## References

[1] https://www.healtheffects.org/announcements/state-global-air-2018-over-7-billion-people-face-unsafe-air (Accessed 12 September 2018).
[2] M. Amann, M. Lutz, The revision of the air quality legislation in the European Union related to ground-level ozone, J. Hazard. Mater. 78 (2000) 41–62.
[3] http://www.who.int/ipcs/features/benzene.pdf (Accessed 12 September 2018).
[4] W.B. Li, J.X. Wang, H. Gong, Catalytic combustion of VOCs on non-noble metal catalysts, Catal. Today 148 (2009) 81–87.
[5] H. Deng, S. Kang, J. Ma, C. Zhang, H. Hong, Silver incorporated into cryptomelane-type Manganese oxide boosts the catalytic oxidation of benzene, Appl. Catal. B: Environ. 239 (2018) 214–222.
[6] S.C. Kim, W.G. Shim, Properties and performance of Pd based catalysts for catalytic oxidation of volatile organic compounds, Appl. Catal. B: Environ. 92 (2009) 429–436.
[7] C. He, J. Li, P. Li, J. Cheng, Z. Hao, Z.P. Xu, Comprehensive investigation of Pd/ZSM-5/MCM-48 composite catalysts with enhanced activity and stability for benzene oxidation, Appl. Catal. B: Environ. 96 (2010) 466–475.
[8] Y. Liu, H. Dai, J. Deng, S. Xie, H. Yang, W. Tan, W. Han, Y. Jiang, G. Guo, Mesoporous $Co_3O_4$-supported gold nanocatalysts: highly active for the oxidation of carbon monoxide, benzene, toluene, and o-xylene, J. Catal. 309 (2014) 408–418.
[9] A.G.M. da Silva, T.S. Rodrigues, T.J.A. Slater, E.A. Lewis, R.S. Alves, H.V. Fajardo, R. Balzer, A.H.M. da Silva, I.C. de Freitas, D.C. Oliveira, J.M. Assaf, L.F.D. Probst, S.J. Haigh, P.H.C. Camargo, Controlling size, morphology, and surface composition of AgAu nanodendrites in 15 s for improved environmental catalysis under low metal loadings, ACS Appl. Mater. Interfaces 7 (2015) 25624–25632.
[10] Y. Chen, Z. Huang, M. Zhou, Z. Ma, J. Chen, X. Tang, Single silver adatoms on nanostructured manganese oxide surfaces: boosting oxygen activation for benzene abatement, Environ. Sci. Technol. 51 (2017) 2304–2311.
[11] S.C. Kim, The catalytic oxidation of aromatic hydrocarbons over supported metal oxide, J. Hazard. Mater. B91 (2002) 285–299.
[12] D.P. Debecker, K. Bouchmella, R. Delaigle, P. Eloy, C. Poleunis, P. Bertrand, E.M. Gaigneaux, P.H. Mutin, One-step non-hydrolytic sol-gel preparation of efficient $V_2O_5$-$TiO_2$ catalysts for VOC total oxidation, Appl. Catal. B: Environ. 94 (2010) 38–45.
[13] D.P. Debecker, R. Delaigle, K. Bouchmella, P. Eloy, E.M. Gaigneaux, P.H. Mutin, Total oxidation of benzene and chlorobenzene with $MoO_3$- and $WO_3$-promoted $V_2O_5$/$TiO_2$ catalysts prepared by a nonhydrolytic sol-gel route, Catal. Today 157 (2010) 125–130.
[14] S.C. Kim, W.G. Shim, Catalytic combustion of VOCs over a series of manganese oxide catalysts, Appl. Catal. B: Environ. 98 (2010) 180–185.
[15] T.Y. Li, S.J. Chiang, B.J. Liaw, Y.Z. Chen, Catalytic oxidation of benzene over CuO/$Ce_{1-x}Mn_xO_2$ catalysts, Appl. Catal. B: Environ. 103 (2011) 143–148.
[16] L.Pdos S. Xavier, V. Rico-Pérez, A.M. Hernández-Giménez, D. Lozano-Castelló, A. Bueno-López, Simultaneous catalytic oxidation of carbon monoxide, hydrocarbons and soot with Ce-Zr-Nd mixed oxides in simulated diesel exhaust conditions, Appl. Catal. B: Environ. 162 (2015) 412–419.
[17] H. Huang, Y. Xu, Q. Feng, D.Y.C. Leung, Low temperature catalytic oxidation of volatile organic compounds: a review, Catal. Sci. Technol. 5 (2015) 2649–2669.
[18] J.E. Post, Manganese oxide minerals: crystal structures and economic and environmental significance, Proc. Natl. Acad. Sci. U. S. A. 96 (1999) 3447–3454.
[19] S. Grangeon, A. Manceau, J. Guilhermet, A.C. Gaillot, M. Lanson, B. Lanson, Zn sorption modifies dynamically the layer and interlayer structure of vernadite, Geochim. Cosmochim. Ac. 85 (2012) 302–313.
[20] M. Zeng, Y. Li, F. Liu, Y. Yang, M. Mao, X. Zhao, Cu doped OL-1 nanoflower: A UV-vis-infrared light-driven catalystfor gas-phase environmental purification with very high efficiency, Appl. Catal. B: Environ. 200 (2017) 521–529.
[21] L. Zhu, J. Wang, S. Rong, H. Wang, P. Zhang, Cerium modified birnessite-type $MnO_2$ for gaseous formaldehyde oxidation at low temperature, Appl. Catal. B: Environ. 211 (2017) 212–221.
[22] G.G. Yadav, J.W. Gallaway, D.E. Turney, M. Nyce, J. Huang, X. Wei, S. Banerjee, Regenerable Cu-intercalated $MnO_2$ layered cathode for highly cyclable energy dense batteries, Nat. Commun. 8 (2017) 14424–14432.
[23] Y. Liu, W. Yang, P. Zhang, J. Zhang, Nitric acid-treated birnessite-type $MnO_2$: An efficient and hydrophobic material for humid ozone decomposition, Appl. Surf. Sci. 442 (2018) 640–649.
[24] F. Liu, S. Rong, P. Zhang, L. Gao, One-step synthesis of nanocarbon-decorated $MnO_2$ with superior activity for indoor formaldehyde removal at room temperature, Appl. Catal. B: Environ. 235 (2018) 158–167.
[25] J. Hou, Y. Li, M. Mao, L. Ren, X. Zhao, Tremendous effect of the morphology of birnessite-type manganese oxide nanostructures on catalytic activity, ACS Appl. Mater. Interfaces 6 (2014) 14981–14987.
[26] Q. Ye, H. Lu, J. Zhao, S. Cheng, T. Kang, D. Wang, H. Dai, A comparative investigation on catalytic oxidation of CO, benzene, and toluene over birnessites derived from different routes, Appl. Surf. Sci. 317 (2014) 892–901.
[27] D. Li, W. Li, Y. Deng, X. Wu, N. Han, Y. Chen, Effective Ti doping of $\delta$-$MnO_2$ via anion route for highly active catalytic combustion of benzene, J. Phys. Chem. C 120 (2016) 10275–10282.
[28] Y. Liu, W. Zong, H. Zhou, D. Wang, R. Cao, J. Zhan, L. Liu, B.W.-L. Jang, Tuning the interlayer cations of birnessite-type $MnO_2$ to enhance its oxidation ability for gaseous benzene with water resistance, Catal. Sci. Technol. 8 (2018) 5344–5358.
[29] J. Jia, P. Zhang, L. Chen, Catalytic decomposition of gaseous ozone over manganese dioxides with different crystal structures, Appl. Catal. B: Environ. 189 (2016) 210–218.
[30] Y. Liu, P. Zhang, Removing surface hydroxyl groups of Ce-modified $MnO_2$ to significantly improve its stability for gaseous ozone decomposition, J. Phys. Chem. C 121 (2017) 23488–23497.
[31] Y. Liu, P. Zhang, Catalytic decomposition of gaseous ozone over todorokite-type manganese dioxides at room temperature: effects of cerium modification, Appl. Catal. A: Gen. 530 (2017) 102–110.
[32] F. Thevenet, L. Olivier, F. Batault, L. Sivachandiran, N. Locoge, Acetaldehyde adsorption on $TiO_2$: influence of $NO_2$ preliminary adsorption, Chem. Eng. J. 281 (2015) 126–133.
[33] F. Lin, Z. Wang, Q. Ma, Y. Yang, R. Whiddon, Y. Zhu, K. Cen, Catalytic deep oxidation of NO by ozone over $MnO_x$ loaded sphericalalumina catalyst, Appl. Catal. B: Environ. 198 (2016) 100–111.
[34] W. Tang, X. Wu, D. Li, Z. Wang, G. Liu, H. Liu, Y. Chen, Oxalate route for promoting activity of manganese oxide catalysts in total VOCs' oxidation: effect of calcination temperature and preparation method, J. Mater. Chem. A Mater. Energy Sustain. 2 (2014) 2544–2554.
[35] J. Chen, X. Chen, X. Chen, W. Xu, Z. Xu, H. Jia, J. Chen, Homogeneous introduction of $CeO_y$ into $MnO_x$-based catalyst for oxidation of aromatic VOCs, Appl. Catal. B: Environ. 224 (2018) 825–835.
[36] S. Li, H. Wang, W. Li, X. Wu, W. Tang, Y. Chen, Effect of Cu substitution on promoted benzene oxidation over porous CuCo-based catalysts derived from layered double hydroxide with resistance of water vapor, Appl. Catal. B: Environ. 166–167 (2015) 260–269.
[37] W. Tang, X. Wu, S. Li, X. Shan, G. Liu, Y. Chen, Co-nanocasting synthesis of mesoporous Cu-Mn composite oxides and their promoted catalytic activities for gaseous benzene removal, Appl. Catal. B: Environ. 162 (2015) 110–121.
[38] S. Mo, S. Li, W. Li, J. Li, J. Chen, Y. Chen, Excellent low temperature performance for total benzene oxidation over mesoporous CoMnAl composited oxides from hydrotalcites, J. Mater. Chem. A 4 (2016) 8113–8122.
[39] S. Mo, S. Li, J. Li, Y. Deng, S. Peng, J. Chen, Y. Chen, Rich surface Co(III) ions-enhanced Co nanocatalyst benzene/toluene oxidation performance derived from $Co^{II}Co^{III}$ layered double hydroxide, Nanoscale 8 (2016) 15763–15773.
[40] V.B.R. Boppana, S. Yusuf, G.S. Hutchings, F. Jiao, Nanostructured alkaline-cation-containing $\delta$-$MnO_2$ for photocatalytic water oxidation, Adv. Funct. Mater. 23 (2013) 878–884.
[41] P.J. Ollivier, T.E. Mallouk, A "Chimie Douce" sythesis of perovskite-type $SrTa_2O_6$ and $SrTa_{2-x}Nb_xO_6$, Chem. Mater. 10 (1998) 2585–2587.
[42] T. Wang, Y. Sun, Y. Zhou, S. Sun, X. Hu, Y. Dai, S. Xi, Y. Du, Y. Yang, Z.J. Xu, Identifying influential parameters of octahedrally coordinated cations in spinel $ZnMn_xCo_{2-x}O_4$ oxides for the oxidation reaction, ACS Catal. 8 (2018) 8568–8577.
[43] J.W. Murray, J.G. Dillard, R. Giovanoli, H. Moers, W. Stumm, Oxidation of Mn(II): Initial mineralogy, oxidation state and ageing, Geochim. Cosmochim. Ac. 49 (1985) 463–470.
[44] Y. Liu, P. Zhang, J. Zhan, L. Liu, Heat treatment of $MnCO_3$: an easy way to obtain efficient and stable $MnO_2$ for humid $O_3$ decomposition, Appl. Surf. Sci. 463 (2019) 374–385.
[45] Y. Yang, Y. Li, M. Zeng, M. Mao, L. Lan, H. Liu, J. Chen, X. Zhao, UV-vis-infrared light-driven photothermocatalytic abatement of CO on Cu doped ramsdellite $MnO_2$ nanosheets enhanced by a photoactivation effect, Appl. Catal. B: Environ. 224 (2018) 751–760.
[46] P. Venkataswamy, K.N. Rao, D. Jampaiah, B.M. Reddy, Nanostructured manganese doped ceria solid solutions for CO oxidation at lower temperatures, Appl. Catal. B: Environ. 162 (2015) 122–132.
[47] Z. Ye, J.-M. Giraudon, N. Nuns, P. Simon, N. De Geyter, R. Morent, J.-F. Lamonier, Influence of the preparation method on the activity of copper-manganese oxides for toluene total oxidation, Appl. Catal. B: Environ. 223 (2018) 154–166.
[48] P. Yang, S. Yang, Z. Shi, Z. Meng, R. Zhou, Deep oxidation of chlorinated VOCs over

$CeO_2$-based transition metal mixed oxide catalysts, Appl. Catal. B: Environ. 162 (2015) 227–235.
[49] J. Chen, X. Chen, W. Xu, Z. Xu, J. Chen, H. Jia, J. Chen, Hydrolysis driving redox reaction to synthesize Mn-Fe binary oxides as highly active catalysts for the removal of toluene, Chem. Eng. J. 330 (2017) 281–293.
[50] X. Chen, X. Chen, S. Cai, J. Chen, W. Xu, H. Jia, J. Chen, Catalytic combustion of toluene over mesoporous $Cr_2O_3$-supported platinum catalysts prepared by *in situ* pyrolysis of MOFs, Chem. Eng. J. 334 (2018) 768–779.
[51] X. Weng, P. Sun, Y. Long, Q. Meng, Z. Wu, Catalytic oxidation of chlorobenzene over $Mn_xCe_{1-x}O_2$/HZSM-5 catalysts: a study with practical implications, Environ. Sci. Technol. 51 (2017) 8057–8066.
[52] B. de Rivas, R. López-Fonseca, J.R. González-Velasco, J.I. Gutiérrez-Ortiz, On the mechanism of the catalytic destruction of 1,2-dichloroethane over Ce/Zr mixed oxide catalysts, J. Mol. Catal. A Chem. 278 (2007) 181–188.
[53] K.T. Wan, C.B. Khouw, M.E. Davis, Studies on the catalytic activity of zirconia promoted with sulfate, iron, and manganese, J. Catal. 158 (1996) 311–326.
[54] A. Biabani-Ravandi, M. Rezaei, Z. Fattah, Low-temperature CO oxidation over nanosized Fe-Co mixed oxide catalysts: effect of calcination temperature and operational conditions, Chem. Eng. Sci. 94 (2013) 237–244.
[55] S. Xing, C. Hu, J. Qu, H. He, M. Yang, Characterization and reactivity of $MnO_x$ supported on mesoporous zirconia for herbicide 2,4-D mineralization with ozone, Environ. Sci. Technol. 42 (2008) 3363–3368.
[56] P. Mars, D.W. van Krevelen, Oxidations carried out by means of vanadium oxide catalysts, Chem. Eng. Sci. 3 (Suppl. 1) (1954) 41–59.
[57] L. Lukashuk, N. Yigit, R. Rameshan, E. Kolar, D. Teschner, M. Hävecker, A. Knop-Gericke, R. Schlögl, K. Föttinger, G. Rupprechter, Operando insights into CO oxidation on cobalt oxide catalysts by NAP-XPS, FTIR, and XRD, ACS Catal. 8 (2018) 8630–8641.
[58] X. Xu, L. Li, J. Huang, H. Jin, X. Fang, W. Liu, N. Zhang, H. Wang, X. Wang, Engineering $Ni^{3+}$ cations in NiO lattice at the atomic level by $Li^+$ doping: the roles of $Ni^{3+}$ and oxygen species for CO oxidation, ACS Catal. 8 (2018) 8033–8045.
[59] V. Mehar, M. Kim, M. Shipilin, M.V. den Bossche, J. Gustafson, L.R. Merte, U. Hejral, H. Grönbeck, E. Lundgren, A. Asthagiri, J.F. Weaver, Understanding the intrinsic surface reactivity of single-layer and multilayer PdO(101) on Pd(100), ACS Catal. 8 (2018) 8553–8567.
[60] J. Wang, X. Wang, X. Liu, T. Zhu, Y. Guo, H. Qi, Catalytic oxidation of chlorinated benzenes over $V_2O_5$/$TiO_2$ catalysts: the effects of chlorine substituents, Catal. Today 241 (2015) 92–99.
[61] A. Corma, H. García, Lewis acids as catalysts in oxidation reactions: from homogeneous to heterogeneous systems, Chem. Rev. 102 (2002) 3837–3892.
[62] J. Wang, G. Zhang, P. Zhang, Layered birnessite-type $MnO_2$ with surface pits for enhanced catalytic formaldehyde oxidation activity, J. Mater. Chem. A 5 (2017) 5719–5725.
[63] J. Wang, G. Zhang, P. Zhang, Graphene-assisted photothermal effect on promoting catalytic activity of layered $MnO_2$ for gaseous formaldehyde oxidation, Appl. Catal. B: Environ. 239 (2018) 77–85.
[64] B. Liu, C. Li, G. Zhang, X. Yao, S.T.C. Chuang, Z. Li, Oxygen vacancy promoting dimethyl carbonate synthesis from $CO_2$ and methanol over Zr-doped $CeO_2$ nanorods, ACS Catal. 8 (2018) 10446–10456.